Autonomous Robots 15, 111–127, 2003

Learning Occupancy Grid Maps with Forward Sensor Models

SEBASTIAN THRUN
Computer Science Department, Stanford University, Stanford, CA 94305, USA
thrun@stanford.edu

Abstract. This article describes a new algorithm for acquiring occupancy grid maps with mobile robots. Existing occupancy grid mapping algorithms decompose the high-dimensional mapping problem into a collection of one-dimensional problems, where the occupancy of each grid cell is estimated independently. This induces conflicts that may lead to inconsistent maps, even for noise-free sensors. This article shows how to solve the mapping problem in the original, high-dimensional space, thereby maintaining all dependencies between neighboring cells. As a result, maps generated by our approach are often more accurate than those generated using traditional techniques. Our approach relies on a statistical formulation of the mapping problem using forward models. It employs the expectation maximization algorithm for searching maps that maximize the likelihood of the sensor measurements.

Keywords: mobile robotics, mapping, Bayesian techniques, probabilistic inference, robot navigation, SLAM

1. Introduction

In the past two decades, occupancy grid maps have become a dominant paradigm for environment modeling in mobile robotics. Occupancy grid maps are spatial representations of robot environments. They represent environments by fine-grained, metric grids of variables that reflect the occupancy of the environment. Once acquired, they enable various key functions necessary for mobile robot navigation, such as localization, path planning, collision avoidance, and people finding.

The basic occupancy grid map paradigm has been applied successfully in many different ways. For example, some systems use maps locally, to plan collision-free paths or to identify environment features for localization (Borenstein and Koren, 1991; Konolige and Chou, 1999; Schiele and Crowley, 1994; Simmons, 1996). Others, such as many of the systems described in Kortenkamp et al. (1998) and Thrun (1998), rely on global occupancy grid maps for global path planning and navigation. Occupancy maps have been built using sonar sensors (Moravec and Elfes, 1985; Yamauchi, 1997), laser range finders (Thrun, 1998), and stereo vision (Buhmann, 1995; Moravec and Martin, 1994; Murray and Little, 2001). While most existing occupancy mapping algorithms use two-dimensional maps, some actually develop three-dimensional, volumetric maps (Moravec and Martin, 1994). Various authors have investigated building such maps while simultaneously localizing the robot (Burgard, 1999; Thrun, 1998; Yamauchi et al., 1998) and during robot exploration (Burgard, 2000; Simmons et al., 2000; Thrun, 1993; Yamauchi, 1997). Some authors have extended occupancy grid maps to contain enriched information, such as information pertaining to the reflective properties of the surface materials (Howard and Kitchen, 1996). Occupancy grid maps are arguably the most successful environment representation in mobile robotics to date (Kortenkamp et al., 1998).

Existing occupancy grid mapping algorithms suffer a key problem. They often generate maps that are inconsistent with the data, particularly in cluttered environments. This problem is due to the fact that existing algorithms decompose the high-dimensional mapping problem into many one-dimensional estimation problems—one for each grid cell—which are then tackled independently. The problem is common in environments like the one shown in Fig. 1, where a moving robot passes by an open door. Under conventional occupancy grid mapping algorithms, the sonar measurements are conflicting with one another in the region of

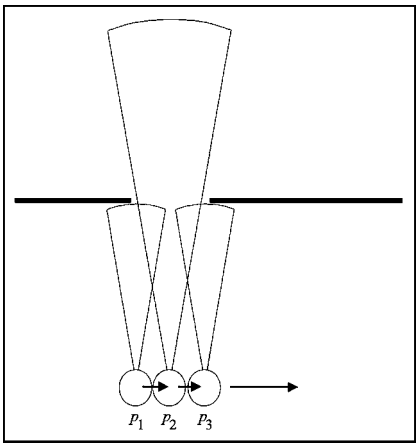

Figure 1. A set of noise-free sonar measurements that a robot may receive while passing an open door. While the measurements are perfectly consistent, existing occupancy grid maps induce a conflict in the door region, where short and long sensor cones overlap. This article presents a method that overcomes this problem.

the doorway—which often leads to the doorway being closed in the final map.

Figure 2 illustrates the problem graphically. In diagram (a), a passing robot might receive the (noise-free) range measurements shown in diagram (b). Inverse sensor models map these beams into probabilistic maps. This is done separately for each grid cell and each beam, as shown in diagrams (c) and (d). Combining both interpretations may yield a map as shown in diagram (e). Obviously, there is a conflict in the overlap region, indicated by the circles in this diagram. Such conflicts are usually accommodated by averaging. The interesting insight is: There exist maps, such as the one in diagram (f), which perfectly explains the sensor measurements without any such conflict. This is because for a sensor reading to be explained, it suffices to assume an obstacle *somewhere* in its measurement cone. Put differently, the fact that cones sweep over multiple grid cells induces important dependencies between neighboring grid cells. A decomposition of the mapping problem into thousands of binary estimation problems—as is common practice in the literature—does not consider these dependencies and therefore may yield suboptimal results.

While this consideration uses sonar sensors as motivating example, it is easily extended to certain other sensor types that may be used for building occupancy maps, such as stereo vision (Murray and Little, 2001);

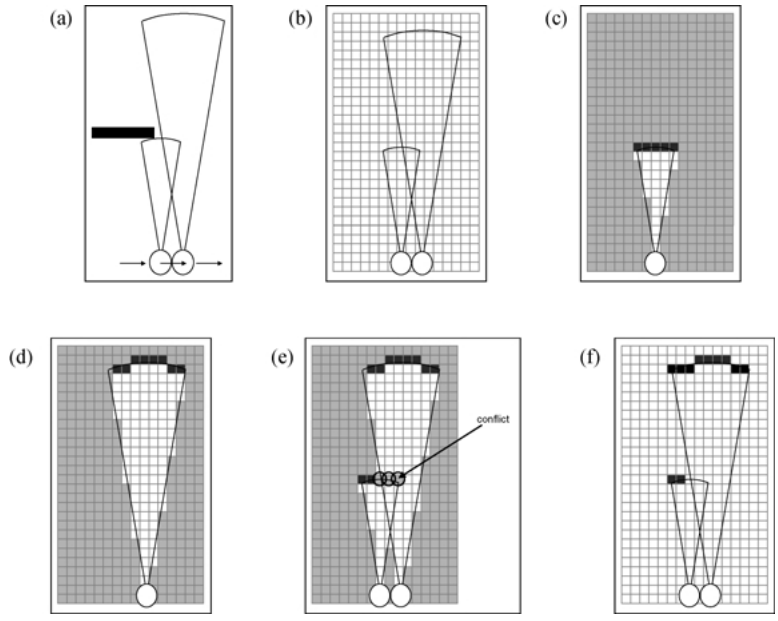

Figure 2. The problem with current occupancy grid mapping algorithms: For the environment shown in (a), a passing robot might receive the (noise-free) measurement shown in (b). Inverse sensor models map these beams into probabilistic maps. This is done separately for each grid cell and each beam, as shown in (c) and (d). Combining both interpretations may yield a map as shown in (e). Obviously, there is a conflict in the overlap region, indicated by the circles in (e). The interesting insight is: There exist maps, such as the one in diagram (f), which perfectly explain the sensor measurement without any such conflict. For a sensor reading to be explained, it suffices to assume an obstacle *somewhere* in the cone of a measurement, and not everywhere. This effect is captured by the forward models described in this article.

it is, however, less applicable to laser range finders, due to their relatively small angular perceptual field. This article derives an alternative algorithm, which solves the mapping problem in the original, high-dimensional space (Thrun, 2001). In particular, our approach formulates the mapping problem as a maximum likelihood problem in a high-dimensional space, often with tens of thousands of dimensions. The estimation is carried out using the *expectation maximization algorithm* (in short: EM) (Dempster et al., 1977). A key feature of our approach is that it relies on forward probabilistic models of sensors, which model the physics of sensors. This is in contrast to the literature on occupancy grid mapping, which typically uses inverse models for interpreting sensor measurements. To obtain a probabilistic map with uncertainty, we calculate marginals of the occupancy probability of each grid cell conditioned on the map found by EM. Empirical results show that our approach yields considerably more accurate maps.

2. Occupancy Grid Mapping with Inverse Models

This section establishes the basic mathematical notation and derives the basic occupancy grid mapping approach (Elfes, 1989; Moravec, 1988; Moravec and Martin, 1994). Standard occupancy methods are characterized by two algorithmic choices:

1. They decompose the high-dimensional mapping problem into many binary estimation problems, which are then solved independently of each other.
2. They rely on inverse models of the robot's sensors which reasons from sensor measurements to maps (opposite of the way sensor data is generated).

As discussed in the introduction to this article, this decomposition creates conflicts even for noise-free data. Techniques such as Bayesian reasoning are then employed on the grid cell level to resolve these conflicts. We view this approach as computationally elegant but inferior to methods that treat the mapping problem for what it is: A problem in a high dimensional space.

Let m be the occupancy grid map. We use $m_{x,y}$ to denote the occupancy of the grid cell with index $\langle x, y\rangle$. Occupancy grid maps are estimated from sensor measurements (e.g., sonar measurements). Let $z_1, \ldots, z_T$ denote the measurements from time 1 through time T, along with the pose at which the measurement was taken (which is assumed to be known). For example, z_t might be a sonar scan and a three-dimensional pose variable (x-y coordinates of the robot and heading direction). Each measurement carries information about the occupancy of many grid cells. Thus, the problem addressed by occupancy grid mapping is the problem of determining the probability of occupancy of each grid cell m given the measurements $z_1, \ldots, z_T$:

$$p(m \mid z_1, \ldots, z_T) \tag{1}$$

Maps are defined over high-dimensional spaces. Therefore, this posterior cannot be represented easily. Standard occupancy grid mapping techniques decompose the problem into many one-dimensional estimation problems, which are solved independently of each other. These one-dimensional problems correspond to estimation problems for the individual cells $m_{x,y}$ of the grid:

$$p(m_{x,y} \mid z_1, \ldots, z_T) \tag{2}$$

For computational reasons, it is common practice to calculate the so-called *log-odds* of $p(m_{x,y} \mid z_1, \ldots, z_T)$ instead of estimating the posterior $p(m_{x,y} \mid z_1, \ldots, z_T)$. The log-odds is defined as follows:

$$l^T_{x,y} = \log \frac{p(m_{x,y} \mid z_1, \ldots, z_T)}{1 - p(m_{x,y} \mid z_1, \ldots, z_T)} \tag{3}$$

The log-odds can take on any value in $\Re$. From log-odds $l^T_{x,y}$ defined in (3), it is easy to "recover" the posterior occupancy probability $p(m_{x,y} \mid z_1, \ldots, z_T)$:

$$p(m_{x,y} \mid z_1, \ldots, z_T) = 1 - [1 + e^{l^T - x,y}]^{-1} \tag{4}$$

The log-odds at any point in time t is estimated recursively via Bayes rule, applied to the posterior $p(m_{x,y} \mid z_1, \ldots, z_t)$:

$$p(m_{x,y} \mid z_1, \ldots, z_t) = \frac{p(z_t \mid z_1, \ldots, z_{t-1}, m_{x,y}) p(m_{x,y} \mid z_1, \ldots, z_{t-1})}{p(z_t \mid z_1, \ldots, z_{t-1})} \tag{5}$$

A common assumption in mapping is the *static world assumption*, which states that past sensor readings are conditionally independent given knowledge of the map m, for any point in time t:

$$p(z_t \mid z_1, \ldots, z_{t-1}, m) = p(z_t \mid m) \tag{6}$$

This assumption is valid in static environments with a non-changing map. It will also be made by our approach. However, by virtue of the grid decomposition, occupancy grid maps make a much stronger assumption: They assume conditional independence given knowledge of each individual grid cell $m_{x,y}$, regardless of the occupancy of neighboring cells:

$$p(z_t \mid z_1, \ldots, z_{t-1}, m_{x,y}) = p(z_t \mid m_{x,y}) \tag{7}$$

This is an incorrect assumption even in static worlds, since sensor measurements (e.g., sonar cones) sweep over multiple grid cells, all of which have to be known for obtaining independence. However, this conditional independence assumption is convenient. It allows us to simplify (5) to:

$$p(m_{x,y} \mid z_1, \ldots, z_t) = \frac{p(z_t \mid m_{x,y}) p(m_{x,y} \mid z_1, \ldots, z_{t-1})}{p(z_t \mid z_1, \ldots, z_{t-1})} \tag{8}$$

Applying Bayes rule to the term $p(z_t \mid m_{x,y})$ gives us:

$$p(m_{x,y} \mid z_1, \ldots, z_t) = \frac{p(m_{x,y} \mid z_t) p(z_t) p(m_{x,y} \mid z_1, \ldots, z_{t-1})}{p(m_{x,y}) p(z_t \mid z_1, \ldots, z_{t-1})} \tag{9}$$

This equation computes the probability that $m_{x,y}$ is occupied.

A completely analogous derivation leads to the posterior probability that the grid cell $m_{x,y}$ is free. Freeness will be denoted $\bar{m}_{x,y}$:

$$p(\bar{m}_{x,y} \mid z_1, \ldots, z_t) = \frac{p(\bar{m}_{x,y} \mid z_t) p(z_t) p(\bar{m}_{x,y} \mid z_1, \ldots, z_{t-1})}{p(\bar{m}_{x,y}) p(z_t \mid z_1, \ldots, z_{t-1})} \tag{10}$$

By dividing (9) by (10), we can eliminate several hard-to-compute terms:

$$\frac{p(m_{x,y} \mid z_1, \ldots, z_t)}{p(\bar{m}_{x,y} \mid z_1, \ldots, z_t)} = \frac{p(m_{x,y} \mid z_t)}{p(\bar{m}_{x,y} \mid z_t)} \frac{p(\bar{m}_{x,y})}{p(m_{x,y})} \times \frac{p(m_{x,y} \mid z_1, \ldots, z_{t-1})}{p(\bar{m}_{x,y} \mid z_1, \ldots, z_{t-1})} \tag{11}$$

This expression is actually in the form of an odds ratio. To see, we notice that $p(\bar{m}_{x,y}) = 1 - p(m_{x,y})$, and $p(\bar{m}_{x,y} \mid \cdot) = 1 - p(m_{x,y} \mid \cdot)$ for any conditioning variable "$\cdot$". In other words, we can re-write (11) as follows:

$$\frac{p(m_{x,y} \mid z_1, \ldots, z_t)}{1 - p(m_{x,y} \mid z_1, \ldots, z_t)} = \frac{p(m_{x,y} \mid z_t)}{1 - p(m_{x,y} \mid z_t)} \times \frac{1 - p(m_{x,y})}{p(m_{x,y})} \frac{p(m_{x,y} \mid z_1, \ldots, z_{t-1})}{1 - p(m_{x,y} \mid z_1, \ldots, z_{t-1})} \tag{12}$$

The desired log-odds is the logarithm of this expression:

$$\log \frac{p(m_{x,y} \mid z_1, \ldots, z_t)}{1 - p(m_{x,y} \mid z_1, \ldots, z_t)} = \log \frac{p(m_{x,y} \mid z_t)}{1 - p(m_{x,y} \mid z_t)} + \log \frac{1 - p(m_{x,y})}{p(m_{x,y})} + \log \frac{p(m_{x,y} \mid z_1, \ldots, z_{t-1})}{1 - p(m_{x,y} \mid z_1, \ldots, z_{t-1})} \tag{13}$$

By substituting in the log-odds $l^t_{x,y}$ as defined above, we arrive at the recursive equation:

$$l^t_{x,y} = \log \frac{p(m_{x,y} \mid z_t)}{1 - p(m_{x,y} \mid z_t)} + \log \frac{1 - p(m_{x,y})}{p(m_{x,y})} + l^{t-1}_{x,y} \tag{14}$$

with the initialization

$$l^0_{x,y} = \log \frac{p(m_{x,y})}{p(1 - m_{x,y})} \tag{15}$$

We note that the calculation of the log-odds can also be written in closed form, by solving the induction over t:

$$l^T_{x,y} = (T - 1) \log \frac{1 - p(m_{x,y})}{p(m_{x,y})} + \sum_{t=1}^{T} \log \frac{p(m_{x,y} \mid z_t)}{1 - p(m_{x,y} \mid z_t)} \tag{16}$$

Table 1 lists the resulting algorithm. The algorithm first initializes a map, then incorporates the sensor readings incrementally. Finally, the desired posteriors are recovered from the log-odds representation of the map.

Equations (14) and (15) are of central importance in occupancy grid mapping. As these equations and the algorithm shown in Table 1 suggest, only two probabilities are needed to implement occupancy grid maps. First, the probability $p(m_{x,y})$, which is the *prior* for occupancy. It is commonly set to a value between 0.2 and 0.5, depending on the expected obstacle density in typical robot environments.

Table 1. The standard occupancy grid mapping algorithm, shown here using log-odds representations.

Algorithm StandardOccGrids(Z):

/ Initialization */*

for all grid cells $\langle x, y \rangle$ *do*

$l_{x,y} = \log p(m_{x,y}) - \log[1 - p(m_{x,y})]$

endfor

/ Grid calculation using log-odds */*

for all time steps t from 1 to T do

for all grid cells $\langle x, y \rangle$ *in the perceptual range of* z_t *do*

$l_{x,y} = l_{x,y} + \log p(m_{x,y} \mid z_t) - \log[1 - p(m_{x,y} \mid z_t)] - \log p(m_{x,y}) + \log[1 - p(m_{x,y})]$

endfor

endfor

/ Recovery of occupancy probabilities */*

for all grid cells $\langle x, y \rangle$ *do*

$p(m_{x,y} \mid z_1, \ldots, z_T) = 1 - \frac{1}{e^{l_{x,y}}}$

endfor

More important is the probability

$$p(m_{x,y} \mid z) \tag{17}$$

which specifies the probability of occupancy of the grid cell $m_{x,y}$ conditioned on the measurement z. This probability constitutes an *inverse sensor model*, since it maps sensor measurements back to its causes. Occupancy grid maps commonly rely on such inverse models. Notice that the inverse model does not take the occupancy of neighboring cells into account: It makes the crucial independence assumption that the occupancy of a cell can be predicted regardless of a cell's neighbors. Herein lies a major problem of the standard occupancy approach, which leads to the phenomena discussed in the introduction to this article. In fact, the problem is common to *any* occupancy mapping algorithm that updates grid cells independently, regardless whether the update is multiplicative, additive, or of any other form.

3. Occupancy Grid Mapping with Forward Models

This section presents our alternative approach to computing occupancy grid maps. The key idea is to use forward models in place of the inverse models discussed in the previous section. Forward models enable us to calculate the likelihood of the sensor measurements for each map and set of robot poses, in a way that considers all inter-cell dependencies. Mapping, thus, becomes an optimization problem, which is the problem of finding the map that maximizes the data likelihood. This optimization problem can be carried out in the original high-dimensional space of all maps, hence does not require the same decomposition into grid cell-specific problems found in the standard occupancy grid mapping literature.

3.1. Forward Model: Intuitive Description

A forward model is a generative description of the physics of the sensors. Put probabilistically, a forward model is of the form

$$p(z \mid m) \tag{18}$$

where z is a sensor measurement and m is the map. In other words, a forward model specifies a probability distribution over sensor measurements z *given* a map m. As before, we assume that the robot poses are known and part of z.

The specific forward model used in our implementation is quite simplistic. It models two basic causes of sensor measurements:

1. *The non-random case.* Each occupied cell in the cone of a sensor has a probability p_{hit} of reflecting a sonar beam. If a sonar beam is reflected back into

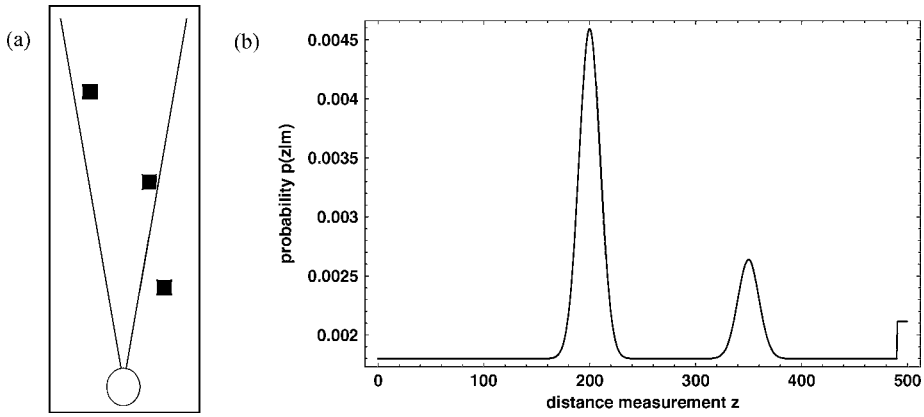

Figure 3. Example of a probabilistic forward model. Diagram (a) depicts a map with three obstacles (dark squares), two of which lie in the sensor cone of a sonar sensor. Diagram (b) depicts the probability of measuring z, for different ranges z. The large peak in diagram (b) corresponds to the nearest obstacle in the cone. The second (smaller) peak corresponds to the obstacle further away, which is only detected if the near obstacle is missed. If neither of the obstacles is detected, the sensor returns a max-range reading, which is indicated by the peak on the far right. Finally, this probability density is mixed with a uniform density that models random measurement errors.

the sensor, the measurement is distorted by Gaussian noise. Of course, the nearest occupied grid cell has the highest probability of being detected, followed by the second nearest, and so on. In other words, the detection probability is distributed according to a geometric distribution with parameter p_{hit}, convolved with Gaussian noise.

2. *The random case.* With probability p_{rand}, a sonar reading is random, drawn from a uniform distribution over the entire measurement range. In our simplistic sensor model, the possibility that a sonar reading is random captures all unmodeled effect, such as specular reflections, spurious readings, etc.

Before formalizing the forward model, let us illustrate it using an example. Figure 3(a) shows a map with three obstacles (dark squares) and a sonar cone. Two of the obstacles overlap with the cone; the other is irrelevant. With probability p_{rand}, the measurement is random. Otherwise, the robot either detects one of the obstacles or receives a max-range measurement. The probability for detecting the nearer of the two obstacles is $(1 - p_{\text{rand}}) \cdot p_{\text{hit}}$; however, with probability $(1 - p_{\text{rand}}) \cdot (1 - p_{\text{hit}})$ the robot fails to detect the near obstacle. It may then detect the second obstacle, which will happen with probability $(1 - p_{\text{rand}}) \cdot (1 - p_{\text{hit}}) \cdot p_{\text{hit}}$. Otherwise, its sensor will have missed both obstacles and return a max-range reading, which happens with probability $(1 - p_{\text{rand}}) \cdot (1 - p_{\text{hit}})^2$.

For the example shown in Fig. 3(a) and (b) shows the corresponding probability density function $p(z \mid m)$. Clearly visible there are two peaks of high probability, corresponding to both obstacles in the cone. Also visible is a third peak at the max-range of the sensor, which models the (rare) case that neither obstacle is detected. Notice that the density function in Fig. 3(b) is mixed with a uniform distribution that models random noise.

Clearly, such a forward model is a simplistic approximation of the true characteristics of sonar sensors. More accurate forward models might model specular reflection and incorporate surface properties in the predictions of returns (Howard and Kitchen, 1996). Such models will inevitably improve accuracy of the resulting maps; in fact, the notion of forward models makes it possible to bring to bear complex physical model of sonar sensors that are much more difficult to leverage in conventional occupancy grid mapping techniques (Brown, 1985). Nevertheless, as we shall see below, even our simplistic model yields results that are significantly more accurate than those obtained by conventional occupancy grid techniques, even with well-tuned inverse models.

3.2. *Forward Model: Formal Description*

Formally, our sensor model is a mixture model. As before, let z_t be the t-th sensor measurement along with the (known) pose of the robot where the sensor measurement was taken. Let K_t the number of obstacles in the sensor cone of the t-th measurement. Using ray

casting, one can calculate the distances to these obstacles. Let

$$D_t = \left\{d_{t,1}, d_{t,2}, \ldots, d_{t,K_t}\right\} \tag{19}$$

denote the distances to these obstacles in increasing order:

$$d_{t,1} \leq d_{t,2} \leq \cdots \leq d_{t,K_t} \tag{20}$$

Clearly, if obstacles were detected reliably and without noise, i.e., $p_{\text{hit}} = 1$, the measurement would be $d_{t,1}$, the distance to the nearest obstacle.

To describe the multiple causes of a sensor measurements z_t, it is necessary to introduce new variables, which we will refer to as *correspondence variables*. For each sensor measurement, we define $K_t + 2$ binary variables:

$$c_t = \left\{c_{t,*}, c_{t,0}, c_{t,1}, c_{t,2}, \ldots, c_{t,K_t}\right\} \tag{21}$$

Each of these variables corresponds to exactly one cause of the measurement z_t. If $c_{t,k}$ is 1 for $1 \leq k \leq K_t$, the measurement is caused by the k-th obstacle in the obstacle list D_t. If $c_{t,0} = 1$, none of the obstacles in the list were detected and the sensor returns a max-range reading. The random variable $c_{t,*}$ corresponds to the case where a measurement was purely random. Thus, for each measurement z_t exactly one of those variables is 1, all others are 0.

Each of these correspondences define a different probability distribution over the sensor measurements z_t. In the case that the k-th obstacle in D_t caused the measurement, that is, $c_{t,k} = 1$, we have a straightforward Gaussian noise variable centered at the range $d_{t,k}$:

$$p(z_t \mid m, c_{t,k} = 1) = \frac{1}{\sqrt{2\pi\sigma^2}} e^{-\frac{1}{2}\frac{(z_t - d_{t,k})^2}{\sigma^2}} \tag{22}$$

Here σ is the variance of the noise. If the measurement is entirely random, we obtain a uniform distribution:

$$p(z_t \mid m, c_{t,*} = 1) = \frac{1}{z_{\max}} \tag{23}$$

where $z_{\max}$ denotes the maximum sensor range. It will be convenient to write this probability as follows:

$$p(z_t \mid m, c_{t,*} = 1) = \frac{1}{\sqrt{2\pi\sigma^2}} e^{-\frac{1}{2}\log\frac{z_{\max}^2}{2\pi\sigma^2}} \tag{24}$$

The advantage of this notation is its similarity to the Gaussian noise case.

Finally, the sensor measurement might be caused by missing all obstacles in the cone, hence becomes a max-range reading. We will describe this by a Gaussian centered on $z_{\max}$:

$$p(z_t \mid m, c_{t,0} = 1) = \frac{1}{\sqrt{2\pi\sigma^2}} e^{-\frac{1}{2}\frac{(z_t - z_{\max})^2}{\sigma^2}} \tag{25}$$

We can now merge all these different causes together into a single likelihood function. Recall that c_t denotes the set of all correspondence variables for the measurement z_t.

$$p(z_t \mid m, c_t) = \frac{1}{\sqrt{2\pi\sigma^2}} e^{-\frac{1}{2}\left[c_{t,*}\log\frac{z_{\max}^2}{2\pi\sigma^2} + \sum_{k=1}^{K_t} c_{t,k}\frac{(z_t - d_{t,k})^2}{\sigma^2} + c_{t,0}\frac{(z_t - z_{\max})^2}{\sigma^2}\right]} \tag{26}$$

Notice that in Eq. (26), exactly one of the correspondence variables in c_t is 1. Thus, for each of those possibilities, this equation reduces to one of the noise models outlined above.

Equation (26) calculates the probability of a sensor measurement z_t if its cause is known, via the correspondence variable c_t. In practice, we are of cause not told what obstacle, if any, was detected. Put differently, the correspondence variables are latent. All we have are range measurements z_t. It is therefore convenient to calculate the *joint* probability over measurements and correspondences c_t, which is obtained as follows:

$$\begin{aligned} p(z_t, c_t \mid m) &= p(z_t \mid m, c_t) p(c_t \mid m) \\ &= p(z_t \mid m, c_t) p(c_t) \end{aligned} \tag{27}$$

Here $p(c_t)$ is the *prior* over correspondences, which describes how likely each possible correspondence is. We already informally described the prior in the previous section, where we argued that the probability of receiving a random reading is p_{rand}, and the probability of detecting an obstacle in the non-random case is p_{hit} for each obstacle in the sensor cone. Put formally, we obtain

$$p(c_t) = \begin{cases} p_{\text{rand}} & \text{if } c_{t,*} = 1 \\ (1 - p_{\text{rand}})(1 - p_{\text{hit}})^{K_t} & \text{if } c_{t,0} = 1 \\ (1 - p_{\text{rand}})(1 - p_{\text{hit}})^{k-1} p_{\text{hit}} & \text{if } c_{t,k} = 1 \text{ for } k \geq 1 \end{cases} \tag{28}$$

which defines the mixture uniform-geometric distribution discussed above.

3.3. Expected Data Log-Likelihood

To find the most likely map, we now have to define the data likelihood. In accordance with the statistical literature, we will define the log-likelihood of the data, exploiting the observation that maximizing the log-likelihood is equivalent to maximizing the likelihood (the logarithm is strictly monotonic).

First, let us define the probability of *all* data. Above, we formulated the probability of a single measurement z_t. As above, our approach makes a static world assumption, but it does not make the strong independence assumption of the standard occupancy grid mapping approach discussed above. This enables us to write the likelihood of all data and correspondences as the following product:

$$p(Z, C \mid m) = \prod_t p(z_t, c_t \mid m) \tag{29}$$

Here Z denotes the set of all measurements (including poses), and C is the set of all correspondences c_t for all data. The logarithm of this expression is given by

$$\log p(Z, C \mid m) = \sum_t \log p(z_t, c_t \mid m) \tag{30}$$

Finally, we notice that we are not really interested in calculating the probability of the correspondence variables, since those are unobservable. Hence, we integrate those out by calculating the expectations of the log-likelihood:

$$E[\log p(Z, C \mid m) \mid Z, m] \tag{31}$$

Here the expectation E is taken over all correspondence variables. The expected log-likelihood of the data is the function that is being optimized in our approach. We obtain the expected log-likelihood from Eq. (31) by substituting Eqs. (30), (27), and (26), as indicated:

$$\begin{aligned}
&E[\log p(Z, C \mid m) \mid Z, m] \\
&\overset{(30)}{=} E\left\{ \sum_t \log p(z_t, c_t \mid m) \,\middle|\, Z, m \right\} \\
&\overset{(27)}{=} E\left\{ \sum_t \log p(z_t \mid c_t, m) p(c_t) \,\middle|\, Z, m \right\} \\
&\overset{(26)}{=} E\left\{ \sum_t \left[\log p(c_t) + \log \frac{1}{\sqrt{2\pi\sigma^2}} \right.\right. \\
&\quad - \frac{1}{2}\left[c_{t,*} \log \frac{z_{\max}^2}{2\pi\sigma^2} + c_{t,0} \frac{(z_t - z_{\max})^2}{\sigma^2} \right. \\
&\quad \left.\left.\left. + \sum_{k=1}^{K_t} c_{t,k} \frac{(z_t - d_{t,k})^2}{\sigma^2} \right]\right] \,\middle|\, Z, m \right\}
\end{aligned} \tag{32}$$

Exploiting the linearity of the expectation E, we obtain:

$$\begin{aligned}
&E[\log p(Z, C \mid m) \mid Z, m] \\
&= \sum_t \left[E[\log p(c_t) \mid z_t, m] + \log \frac{1}{\sqrt{2\pi\sigma^2}} \right. \\
&\quad - \frac{1}{2}\left[E[c_{t,*} \mid z_t, m] \log \frac{z_{\max}^2}{2\pi\sigma^2} \right. \\
&\quad + E[c_{t,0} \mid z_t, m] \frac{(z_t - z_{\max})^2}{\sigma^2} \\
&\quad \left.\left. + \sum_{k=1}^{K_t} E[c_{t,k} \mid z_t, m] \frac{(z_t - d_{t,k})^2}{\sigma^2} \right]\right]
\end{aligned} \tag{33}$$

The goal of mapping is to maximize this log-likelihood. Obviously, the map m and the expectations $E[c_{t,*} \mid z_t, m]$, $E[c_{t,0} \mid z_t, m]$, and $E[c_{t,k} \mid z_t, m]$ all interact. A common way to optimize functions like the one considered here is the *expectation maximization algorithm* (in short: EM) (Dempster et al., 1977), which will be described in turn. As we will see, most terms in this log-likelihood function can be ignored in the EM solution to this problem.

3.4. Finding Maps via EM

EM is an iterative algorithm that gradually maximizes the expected log-likelihood (McLachlan and Krishnan, 1997; Neal and Hinton, 1998). Initially, EM generates a random map m. It then iterates two steps, an E-step, and an M-step, which stand for *expectation step* and *maximization step*, respectively. In the E-step, the expectations over the correspondences are calculated conditioned on a fixed map. The M-step calculates the most likely map based on these expectations. Iterating both steps leads to a sequence of maps that performs hill climbing in the expected log-likelihood space (McLachlan and Krishnan, 1997; Neal and Hinton, 1998).

In detail, we have:

1. *Initialization*. Maps in EM are discrete: Each grid cell is either occupied or free. There is no notion of uncertainty in the map at this level, since EM finds the most likely map—unlike conventional occupancy grid mapping algorithms, which estimates posteriors. In principle, maps can be initialized randomly. However, we observed empirically that using entirely unoccupied maps as initial maps worked best in terms of convergence speed.
2. *E-step*. For a given map m and measurements and poses Z, the E-step calculates the expectations for the correspondences conditioned on m and Z. These expectations are the probabilities for each of the possible causes of the sensor measurements:

$$\begin{aligned} e_{t,*} &:= E[c_{t,*} \mid z_t, m] \\ &= p(c_{t,*} = 1 \mid m, z_t) \\ &= \frac{1}{p(z_t \mid m)} p(z_t \mid m, c_{t,*} = 1) p(c_{t,*} = 1 \mid m) \\ &= \frac{1}{p(z_t \mid m)} \frac{1}{z_{\max}} p_{\text{rand}} \\ &= \frac{1}{p(z_t \mid m)\sqrt{2\pi\sigma^2}} p_{\text{rand}} \frac{\sqrt{2\pi\sigma^2}}{z_{\max}} \\ &= \eta p_{\text{rand}} \frac{\sqrt{2\pi\sigma^2}}{z_{\max}} \end{aligned} \tag{34}$$

Here we defined

$$\eta = \frac{1}{p(z_t \mid m)\sqrt{2\pi\sigma^2}} \tag{35}$$

As we will see below, the variable η is a factor in every single expectation. In particular, we have for $1 \leq k \leq K_t$:

$$\begin{aligned} e_{t,k} &:= E[c_{t,k} \mid z_t, m] \\ &= p(c_{t,k} = 1 \mid m, z_t) \\ &= \frac{1}{p(z_t \mid m)} p(z_t \mid m, c_{t,k} = 1) p(c_{t,k} = 1 \mid m) \\ &= \frac{1}{p(z_t \mid m)} \frac{1}{\sqrt{2\pi\sigma^2}} e^{-\frac{1}{2}\frac{(z_t - d_{t,k})^2}{\sigma^2}} \\ &\quad \times (1 - p_{\text{rand}})(1 - p_{\text{hit}})^{k-1} p_{\text{hit}} \\ &= \frac{1}{p(z_t \mid m)\sqrt{2\pi\sigma^2}} (1 - p_{\text{rand}})(1 - p_{\text{hit}})^{k-1} \\ &\quad \times p_{\text{hit}} e^{-\frac{1}{2}\frac{(z_t - d_{t,k})^2}{\sigma^2}} \\ &= \eta(1 - p_{\text{rand}})(1 - p_{\text{hit}})^{k-1} p_{\text{hit}} e^{-\frac{1}{2}\frac{(z_t - d_{t,k})^2}{\sigma^2}} \end{aligned} \tag{36}$$

Notice that the normalizer η is the same as in Eq. (34). Finally, we obtain for the correspondence variable $c_{t,0}$:

$$\begin{aligned} e_{t,0} &:= E[c_{t,0} \mid z_t, m] \\ &= p(c_{t,0} = 1 \mid m, z_t) \\ &= \frac{1}{p(z_t \mid m)} p(z_t \mid m, c_{t,0} = 1) p(c_{t,0} = 1 \mid m) \\ &= \frac{1}{p(z_t \mid m)} \frac{1}{\sqrt{2\pi\sigma^2}} e^{-\frac{1}{2}\frac{(z_t - z_{\max})^2}{\sigma^2}} \\ &\quad \times (1 - p_{\text{rand}})(1 - p_{\text{hit}})^{K_t} \\ &= \frac{1}{p(z_t \mid m)\sqrt{2\pi\sigma^2}} (1 - p_{\text{rand}}) \\ &\quad \times (1 - p_{\text{hit}})^{K_t} e^{-\frac{1}{2}\frac{(z_t - z_{\max})^2}{\sigma^2}} \\ &= \eta(1 - p_{\text{rand}})(1 - p_{\text{hit}})^{K_t} e^{-\frac{1}{2}\frac{(z_t - z_{\max})^2}{\sigma^2}} \end{aligned} \tag{37}$$

Notice that below, we will only use the expectations $E[c_{t,k} \mid z_t, m]$. However, the the other two expectations are needed for calculating the normalization constant η. In particular, η can be calculated from (34), (36), and (37) as follows:

$$\begin{aligned} \eta = \Bigg\{ & p_{\text{rand}} \frac{\sqrt{2\pi\sigma^2}}{z_{\max}} + (1 - p_{\text{rand}})(1 - p_{\text{hit}})^{K_t} \\ & \times e^{-\frac{1}{2}\frac{(z_t - z_{\max})^2}{\sigma^2}} + \sum_{k=1}^{K_t} \Bigg[(1 - p_{\text{rand}}) \\ & \times (1 - p_{\text{hit}})^{k-1} p_{\text{hit}} e^{-\frac{1}{2}\frac{(z_t - d_{t,k})^2}{\sigma^2}} \Bigg] \Bigg\}^{-1} \end{aligned} \tag{38}$$

3. *M-step*. The M-step regards all expectations as constant relative to the optimization problem of finding the most likely map. Substituting in the expectations calculated in the E-step, the expected log-likelihood (33) becomes:

$$\begin{aligned} & E[\log p(Z, C \mid m) \mid Z, m] \\ &= \sum_t \Bigg[\text{const.} + \log \frac{1}{\sqrt{2\pi\sigma^2}} - \frac{1}{2} \Bigg[e_{t,*} \log \frac{z_{\max}^2}{2\pi\sigma^2} \\ &\quad + e_{t,0} \frac{(z_t - z_{\max})^2}{\sigma^2} + \sum_{k=1}^{K_t} e_{t,k} \frac{(z_t - d_{t,k})^2}{\sigma^2} \Bigg] \Bigg] \end{aligned} \tag{39}$$

When determining a new map m, all but the last term on this expression can be omitted in the optimization. In particular, the only remaining the model asserts on the expected log-likelihood is through the obstacle ranges $d_{t,k}$, which are calculated using the map. This results in the greatly simplified minimization problem:

$$\sum_t \sum_{k=1}^{K_t} e_{t,k}(z_t - d_{t,k})^2 \rightarrow \min \tag{40}$$

The minimization of this expression is performed by hill climbing in the space of all maps. More specifically, the (discrete) occupancy of individual grid cells is flipped whenever doing so decreases the target function (40). This discrete search is terminated when no additional flipping can further decrease the target function.

Implemented in the straightforward way, this approach can turn occupied grid cells into unoccupied ones in the map, but it cannot do the opposite: turning free cells into occupied one. This is because for free cells, the list of ranges D_t lacks the corresponding distance, and hence no expectation is calculated in the E-step. Our implementation, thus, executes a "mini E-step" for any free grid cell that is evaluated in the M-step. This mini E-step involves setting the cell temporarily to occupied, calculating the expectations of all affected sensor measurements, and subsequently determining the likelihood maximizing map (M-step). As argued below, this can be done efficiently using the appropriate data structures.

Since our approach performs maximization in a finite space, it terminates after finitely many steps. In practice, we found that maximizing (40) takes less than a minute on a low-end PC for the types maps shown in this article. Empirically, we never observed that our algorithm was trapped in a poor local minimum. However, the optimum is not always unique.

3.5. *Calculating the Residual Occupancy Uncertainty*

EM generates a single map, composed of zero-one occupancy values. This map contains no notion of posterior uncertainty. In many applications, it is beneficial to know how *certain* we are in the map. Conventional occupancy grid maps achieve this by calculating the marginal posterior probability $p(m_{x,y} \mid Z)$ for each grid cell, as stated in Eq. (4). Unfortunately, calculating such marginal posteriors is computationally intractable in our more general model. Hence, we have to approximate. The essential idea of our approximation is to condition this marginal on the map obtained by EM. Let $\hat{m}$ denote this map, and $\hat{m}_{-x,y}$ the map $\hat{m}$ without the value for the grid cell $\langle x, y \rangle$. Our approach calculates the following posterior:

$$p(m_{x,y} \mid Z, \hat{m}_{-x,y}) \tag{41}$$

This is the marginal posterior over a grid cell's occupancy assuming that the remaining map has been correctly recovered by EM. Before discussing the implications of this approximation, we note that the probability (41) can be calculated very efficiently. In particular, we note that $p(m_{x,y} \mid Z, \hat{m}_{-x,y})$ depends only on a subset of all measurements, namely those whose measurement cones include the grid cell $\langle x, y \rangle$. Denoting this subset by $Z_{x,y}$, we can calculate the desired marginal as follows:

$$\begin{aligned}
&p(m_{x,y} \mid Z, \hat{m}_{-x,y}) \\
&\quad = p(m_{x,y} \mid Z_{x,y}, \hat{m}_{-x,y}) \\
&\quad = \frac{p(Z_{x,y} \mid m_{x,y}, \hat{m}_{-x,y}) p(m_{x,y} \mid \hat{m}_{-x,y})}{p(Z_{x,y} \mid \hat{m}_{-x,y})} \\
&\quad = \frac{p(Z_{x,y} \mid m_{x,y}, \hat{m}_{-x,y}) p(m_{x,y})}{p(Z_{x,y} \mid m_{x,y}, \hat{m}_{-x,y}) p(m_{x,y}) + p(Z_{x,y} \mid \bar{m}_{x,y}, \hat{m}_{-x,y})(1 - p(m_{x,y}))}
\end{aligned} \tag{42}$$

The terms $p(Z \mid m_{x,y}, \hat{m}_{-x,y})$ and $p(Z \mid \bar{m}_{x,y}, \hat{m}_{-x,y})$ express the likelihood of the measurements under the assumptions that $m_{x,y}$ is occupied, or free, respectively. Below, it shall prove convenient to rewrite (42) as log-odds:

$$\begin{aligned}
&\log \frac{p(m_{x,y} \mid Z, \hat{m}_{-x,y})}{1 - p(m_{x,y} \mid Z, \hat{m}_{-x,y})} \\
&\quad = \log \frac{p(Z_{x,y} \mid m_{x,y}, \hat{m}_{-x,y}) p(m_{x,y})}{p(Z_{x,y} \mid \bar{m}_{x,y}, \hat{m}_{-x,y})(1 - p(m_{x,y}))}
\end{aligned} \tag{43}$$

This log odds ratio is easily calculated from the sensor model (26). Our implementation maintains a list of relevant sensor measurements $Z_{x,y}$ for each grid cell $\langle x, y\rangle$, which makes it possible to calculate the marginals for an entire map in a few seconds, even for the largest map shown in this article.

Clearly, conditioning on the EM map $\hat{m}$ is only an approximation. In particular, it fails to capture the residual uncertainty in the map by (falsely) asserting that the map found by EM is the correct one. As a result, our estimates will be overly confident. To counter this overconfidence, our approach mixes this estimate with the prior for occupancy, using a mixing parameter α. The mixing rule is analogous to the update rule of the log odds ratio in in occupancy grid maps (14):

$$\log \frac{q_{x,y}}{1-q_{x,y}} = \alpha \log \frac{p(m_{x,y} \mid Z, \hat{m}_{-x,y})}{1-p(m_{x,y} \mid Z, \hat{m}_{-x,y})} + (1-\alpha) \log \frac{p(m_{x,y})}{1-p(m_{x,y})} \quad (44)$$

Here $q_{x,y}$ denotes the final approximation of the marginal posterior. Solving this equation for q gives us the following expression:

$$q_{x,y} = 1 - \left[1 + \left(\frac{p(m_{x,y} \mid Z, \hat{m}_{-x,y})}{1-p(m_{x,y} \mid Z, \hat{m}_{-x,y})}\right)^{\alpha} \times \left(\frac{p(m_{x,y})}{1-p(m_{x,y})}\right)^{1-\alpha}\right]^{-1} \quad (45)$$

This approach combines two approximations with opposite error. If $\alpha = 1$, the posterior estimate is given by the the term $p(m_{x,y} \mid Z, \hat{m}_{-x,y})$, This term will overestimate the confidence in the value of $m_{x,y}$. If $\alpha = 0$, the posterior (45) is equivalent to the prior for occupancy $p(m_{x,y})$. This prior underestimates the confidence in the occupancy value, since it ignores the measurements Z. This consideration suggests that an "optimal" α exist for each grid cell, which would provide the best approximation to the posterior probability under our model. However, computing this α is intractable; hence we simply set one by hand.

3.6. The Mapping Algorithm with Forward Models

Table 2 summarizes the final algorithm for learning occupancy grid maps using forward models. The algorithm consists of three parts: The initialization, the EM optimization, and a final step that extracts the uncertainty map.

Our implementation uses an efficient data structure for cross-linking sensor measurements z_t and grid cells $\langle x, y\rangle$. A doubly-linked list makes it possible to match measurements and grid cells highly efficiently, without the necessity to search through long lists of grid coordinates, or sensor measurements. Moreover, when calculating the differences $\Delta_{x,y}$, only terms in the expected log-likelihood are considered that actually depend on the grid cell $\langle x, y\rangle$. By doing so, the inner loops of the algorithm are highly efficient, making it possible to generate maps within less than a minute.

As stated at several locations in this article, the advantage of our new algorithm is that it overcomes a critical independence assumption between neighboring grid cells, commonly made in the existing literature on occupancy grid mapping. On the downside, we note that this new occupancy grid mapping algorithm is *not* incremental. Instead, multiple passes through the data are necessary to find a maximum likelihood map. This is a disadvantage relative to the standard occupancy grid mapping algorithm, which can incorporate data incrementally. However, for moderately sized data sets we found that our algorithm takes less than a minute on a low end PC—which is significantly faster than the process of data collection.

4. Experimental Results

Our approach was successfully applied to learning grid maps using simulated and real robot data. Since localization during mapping is not the focus of the current article, we assumed that pose estimates were available. In the simulator, these were easily obtained. For the real world data, we relied on the concurrent mapping and localization algorithm described in Thrun et al. (1998).

Our main findings are that our approach does a better job resolving conflicts among different range measurements. Those are particularly prevalent in discontinuous environment, such as environment with small openings (doors). They also arise in cases with high degrees of noise, which for example is the case when the walls are smooth. In these environments, the increased existence of conflicts induces a degradation of the standard approach that is not found in our approach. However, our approach does not filter our dynamics (e.g., walking people) as nicely as the conventional approach using inverse models.

Table 2. The new occupancy grid mapping algorithm with forward models.

Algorithm ForwardOccGrids(Z):

/*** *Initialization* ***/

for all grid cells $\langle x, y \rangle$ *do* $m_{x,y} = 0$

/*** *Maximum Likelihood Mapping with EM* ***/

repeat until convergence

/*** *Expectation Step* ***/

for all time steps t from 1 to T do

calculate distances D_t *and* K_t *of occupied cells in m under sensor cone* z_t

$e_{t,*} = p_{\text{rand}} \frac{\sqrt{2\pi\sigma^2}}{z_{\max}}$

$e_{t,0} = (1 - p_{\text{hit}})^{K_t} e^{-\frac{1}{2}\frac{(z_t - z_{\max})^2}{\sigma^2}}$

for all $1 \leq k \leq K_t$ *do* $e_{t,k} = (1 - p_{\text{rand}})(1 - p_{\text{hit}})^{k-1} p_{\text{hit}} e^{-\frac{1}{2}\frac{(z_t - d_{t,k})^2}{\sigma^2}}$

$\eta = [e_{t,*} + \sum_{k=0}^{K_t} e_{t,k}]^{-1}$

for all k in $\{*, 1, 2, \ldots, K_t\}$ *do* $e_{t,k} = \eta e_{t,k}$

endfor

/*** *Maximization Step* ***/

repeat until convergence

for all grid cells $\langle x, y \rangle$ *do*

for occupancy $i = 0$ *to 1 do*

$m_{x,y}^{[i]} = 0$

for all measurements z_t *that overlap with* $\langle x, y \rangle$ *do*

calculate distances D_t *and* K_t *of occupied cells in m with* $m_{x,y} = i$ *under cone* z_t

if $m_{x,y} = 0$ *and* $i = 1$ *then recalculate* $e_{t,k}$ *as specified in E-step*

$m_{x,y}^{[i]} = m_{x,y}^{[i]} + e_{t,k}(z_t - d_{t,k})^2$

endfor

endfor

$\Delta_{x,y} = m_{x,y}^{[1]} - m_{x,y}^{[0]}$

if $\Delta_{x,y} \geq 0$ *then* $m_{x,y} = 1$ *else* $m_{x,y} = 0$

endfor

endrepeat

endrepeat

/*** *Uncertainty Map* ***/

for all grid cells $\langle x, y \rangle$ *do*

$q_{x,y} = 1 - [1 + e^{\alpha\Delta_{x,y}}(\frac{p(m_{x,y})}{1 - p(m_{x,y})})^{1-\alpha}]^{-1}$

endfor

4.1. Simulation Results

Our first experiment relied on simulated data. Simulation was chosen because it enables us to carefully vary certain parameters. In our particular case, we were interested in the minimum number of sensor readings required to detect a narrow open door. Figure 4(a) shows an example data set, gathered in a simulated corridor while driving by an open door. This robot is equipped with a circular array of 24 sonar sensors. While driving by the door, the robot receives n readings of the open door—all other readings reflect the much shorter distance to the door posts. With $n = 1$, the standard occupancy grid map algorithm generates the map shown in Fig. 4(b). Our approach is a well-optimized one that uses various smoothing operations to yield

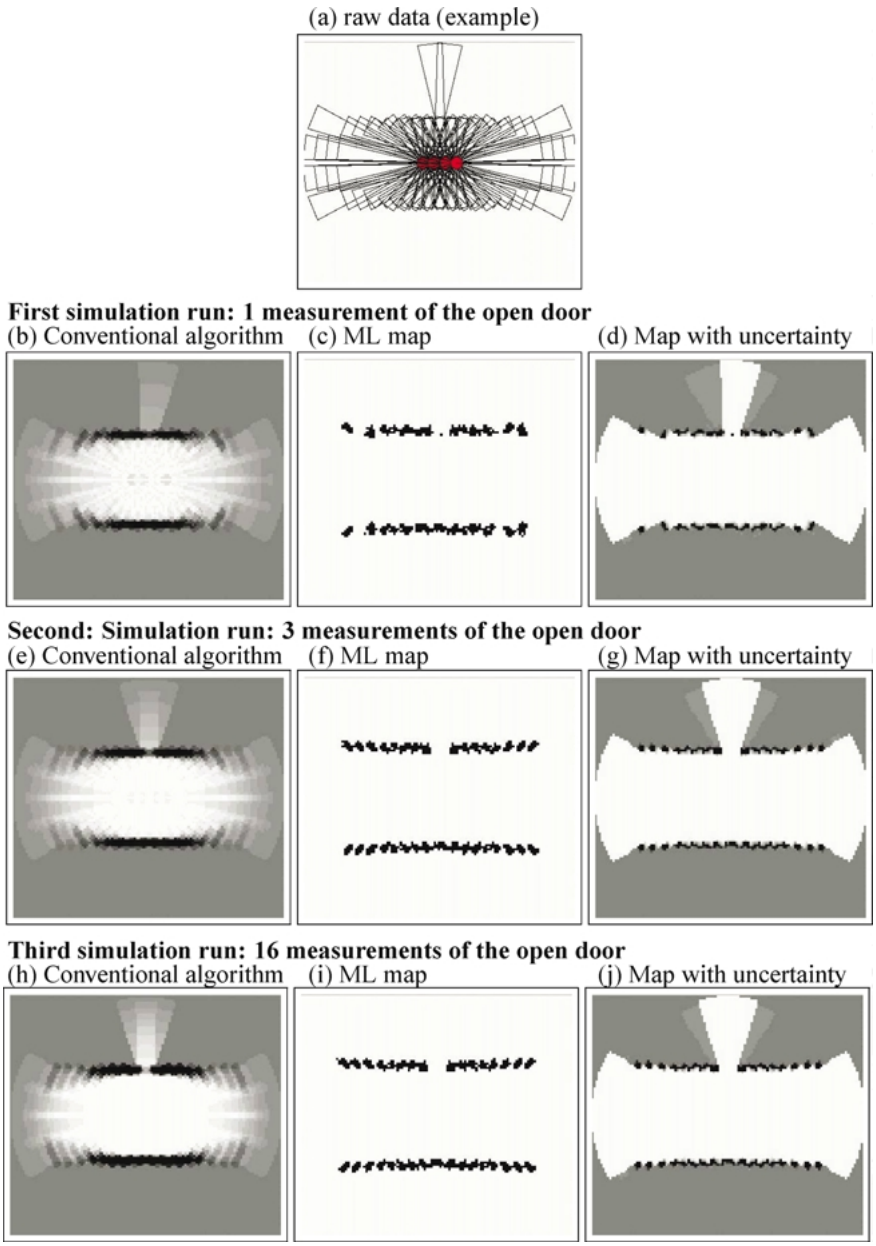

Figure 4. Simulation results: The robot travels along a corridor with an open door. When only a single measurement detects the open door (diagrams (b) through (d)), conventional occupancy grid maps do not show the open door (diagram (b)), whereas our approach does (diagram (d)). The same is the case for a data set where the open door was detected three times (diagrams (e) through (g)). With 16 measurements of the open door, the regular occupancy map show an open door (diagram (h)). Each grid consists of 122 by 107 grid with 10 centimeter resolution.

good occupancy grid maps. Two things are worth noting with respect to Fig. 4(b). First, the open door is mapped wrongly due to the independence assumption in occupancy grid mapping. Second, there are several stripes in the map that are almost perpendicular to the wall. These stripes result from measurements that hit the wall at steep angles.

A maximum likelihood map, found using EM with forward models, is shown Fig. 4(c). Clearly, the most likely solution possesses an open door. In fact, the

result of our algorithm does not attribute any of the sensor reading to a random error event. Instead, all of the sensor readings are perfectly well explained with this map! Figure 4(d) shows the uncertainty map extracted from the maximum likelihood map using our posterior approximation. Again, this map correctly features an open door, confirming our basic conjecture that our approach is superior in handling seemingly inconsistent sensor measurements.

The basic experiment was repeated for different values of n. As n increases, the evidence for an open door increases, and ultimately even the standard occupancy grid mapping algorithm will preclude a map with an open door. The bottom two rows of Fig. 4 show results for $n = 3$, and $n = 16$, respectively. For $n = 3$, the evidence for the existence of an open door is high, yet the standard approach still shows no door, due to the large number of readings that suggest the existence of an obstacle in the door region. Finally, for $n = 16$, the door is visible even for the conventional approach, although not as clearly as for our new approach.

The interesting observation here is while the standard occupancy grid mapping algorithm uses probabilistic means to accommodate inconsistent sensor interpretations, there are no such conflicts in our approach. All data sets are perfectly explained by any of the maximum likelihood maps shown in Fig. 4.

4.2. Real World Results

Real world results were obtained using a RWI B21 robot equipped with 24 sonar sensors, shown in Fig. 5(a). We collected two data sets, both of which possessed unique challenges.

The first data set, documented in Fig. 5(b) and (c), compares the standard occupancy grid mapping algorithm to the one using forward models. In this data set, there are two narrow open doors on either side. As predicted by the simulation, the doors are only visible in the forward modeling approach, whose results are shown in Fig. 5(c). Several dots in the EM map stem from the fact that a person walked by the robot during data collection. This highlights one of the nice features of standard occupancy grid maps, which typically do not show traces of people as long as they do not remain at a single location in the majority of measurements. However, our approach overall a much better job describing the environment.

The final and most interesting data set is much larger. Figure 6(a) shows a robot trace in a 50 meters long corridor. This corridor is quite challenging: On the one hand, there are several open doors on one side. On the other, one of the walls is extremely smooth, resulting in a large number of erroneous readings. The level of noise is so high that the standard occupancy grid approach plainly fails to detect and model the wall, as shown in Fig. 6(b). At the same time, it also fails to detect open doors, as indicated by the arrow in Fig. 6(b). This is interesting, since we have a natural trade-off: By adjusting the gain so as to pay more attention to occupied regions, the wall eventually becomes visible by the doors will be entirely closed. By adjusting the gain into the opposite direction, the doors will eventually become visible but the wall will be missing entirely.

As Fig. 6(c) suggests, our approach succeeds in finding at least some of the wall, while modeling the openings correctly. However, our approach shows the trace of the person controlling the robot with a joystick. The presence of the person violates the static world

Figure 5. (a) The RWI B21 robot used in our experiments. This robot is equipped with a cyclic array of 24 Polaroid sonar sensors. (b) Comparison of conventional occupancy grid mapping with (c) our approach using forward models. The open doors are only visible in (c). However, several small obstacles are shown in (c) that stem from a person walking by the robot during data collection. Each grid consists of 114 by 120 grid with 10 centimeter resolution.

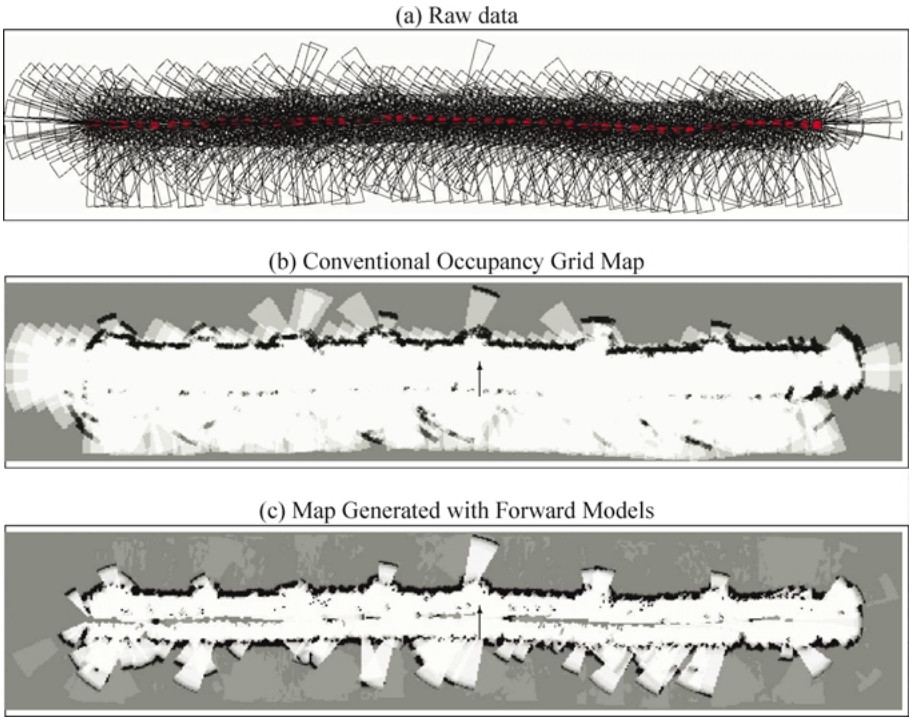

Figure 6. Results obtained for a larger data set, shown in (a). While the wall located at the top of each diagram is easy to detect, the wall shown located below the robot is extremely smooth, producing a large number of erroneous readings. The occupancy grid map shown in (b) doesn't model the wall, while at the same time open doors like the one marked by the arrow are falsely modeled as closed. (c) Forward modeling yields a much improved model of the bottom wall and also models the door correctly. In addition, this map shows a trace of a person walking behind the robot. Each grid consists of 641 by 131 grid with 10 centimeter resolution.

assumption that underlies both families of occupancy grid mapping algorithms; however, our approach generates maps that explain the corresponding readings (but do not look as nice in this regard). Nevertheless, the ability to model both the doors and walls more accurately than the standard approach suggests that our approach is superior in situations with seemingly conflicting range measurements. Generating maps of the size shown here typically takes less than a minute on a low-end PC.

5. Discussion

This article presented an algorithm for generating occupancy grid maps which relies on physical forward models. Instead of breaking down the map learning problem into a multitude of independent binary estimation problems—as is the case in existing occupancy grid mapping algorithms—our approach searches maps in the high-dimensional space. To perform this search, we have adopted the popular EM algorithm to the map estimation problem. The EM algorithm identifies a plausible map by gradually maximizing the likelihood of all measurements in a hill-climbing fashion. Uncertainty maps are obtained by calculating marginal probabilities, similar to those computed by conventional occupancy grid mapping techniques.

Our approach has two main advantages over conventional occupancy grid mapping techniques: First, we believe forward models are more natural to obtain than inverse models, since forward models are descriptive of the physical phenomena that underlie the data generation. Second, and more importantly, our approach yields more consistent maps. This is because our approach relies on fewer independence assumptions. It treats the mapping problem for what it is: A search in a high dimensional space. The disadvantages of our approach are an apparent increased sensitivity to changes in the environment, and a need to go through the data multiple times, which prohibits its real-time application. Extending this algorithm into an online algorithm

is subject of future research (see Neal and Hinton, 1998).

Experimental results illustrate that more accurate maps can be built in situations with seemingly conflicting sensor information. Such situations include environments with narrow openings and environments were sonars frequently fail to detect obstacles. These advantages are counterbalanced by two of the limitations of our approach: First, dynamic obstacles show up more frequently in our approach, and second, our approach is not real-time.

In a recent article (Hähnel et al., 2002), we extended the basic EM approach to accommodate pose uncertainty and environment dynamics. We have successfully demonstrated that the algorithm described here can be extended to yield significantly more accurate maps and robot pose estimates in the presence of moving objects. The key extension here is to include the robot pose variables in the set of latent variables. In the present article, those are obtained through a separate algorithm (Thrun et al., 1998) and simply assumed to be correct. Furthermore, the implementation in Hähnel et al. (2002) employs laser range finders, whose accuracy greatly facilitates the identification of inconsistent sensor measurements when compared to the sonar sensors used in the present article.

As discussed further above, the sensor models used in our implementation are highly simplistic. They do not model many common phenomena in sonar-based range sensing, such as indirect readings caused by specular reflection, or obstacle detection in a sensor's side cone. In principle, the forward modeling approach makes it possible to utilize any probabilistic sensor model, such as the one in Brown (1985). We conjecture that improved sensor models will lead to better mapping results.

Another opportunity for future research arises from the fact that environments possess structure. The prior probability in our approach (and in conventional occupancy grid mapping techniques) assumes independence between different grid cells. In reality, this is just a crude approximation. Environments are usually composed of larger objects, such as walls, furniture, etc. Mapping with forward models facilitate the use of more informed priors, as shown in Liu et al. (2001). However, the acquisition of adequate priors that characterize indoor environments is largely an open research area.

Regardless of these limitations, we believe that our approach sheds light on an alternative approach for building maps with mobile robots. We believe that by overcoming the classical independence that forms the core of techniques based on inverse models, we can ultimately arrive at more powerful mapping algorithms that generate maps of higher consistency with the data. The evidence presented in this and various related papers suggests that forward models are powerful tools for building maps of robot environments.

Acknowledgment

The author thanks Tom Minka, Andrew Y. Ng, and Zoubin Ghahramani for extensive discussions concerning Bayesian approaches and variational approximations for occupancy grid mapping. He also thanks Dirk Hähnel and Wolfram Burgard for discussions on how to apply this approach to SLAM problems in dynamic environments.

This research is sponsored by DARPA's MARS Program (Contract number N66001-01-C-6018 and NBCH1020014) and the National Science Foundation (CAREER grant number IIS-9876136 and regular grant number IIS-9877033), all of which is gratefully acknowledged. The views and conclusions contained in this document are those of the author and should not be interpreted as necessarily representing official policies or endorsements, either expressed or implied, of the United States Government or any of the sponsoring institutions.

References

Borenstein, J. and Koren, Y. 1991. The vector field histogram—fast obstacle avoidance for mobile robots. *IEEE Journal of Robotics and Automation*, 7(3):278–288.

Brown, M.K. 1985. Feature extraction techniques for recognizing solid objects with an ultrasonic range sensor. *IEEE Journal of Robotics and Automation*, RA-1(4).

Buhmann, J., Burgard, W., Cremers, A.B., Fox, D., Hofmann, T., Schneider, F., Strikos, J., and Thrun, S. 1995. The mobile robot Rhino. *AI Magazine*, 16(1).

Burgard, W., Fox, D., Jans, H., Matenar, C., and Thrun, S. 1999. Sonar-based mapping of large-scale mobile robot environments using EM. In *Proceedings of the International Conference on Machine Learning*, Bled, Slovenia.

Burgard, W., Fox, D., Moors, M., Simmons, R., and Thrun, S. 2000. Collaborative multi-robot exploration. In *Proceedings of the IEEE International Conference on Robotics and Automation (ICRA)*, IEEE, San Francisco, CA.

Dempster, A.P., Laird, A.N., and Rubin, D.B. 1977. Maximum likelihood from incomplete data via the EM algorithm. *Journal of the Royal Statistical Society, Series B*, 39(1):1–38.

Elfes, A. 1989. *Occupancy Grids: A Probabilistic Framework for Robot Perception and Navigation*. Ph.D. thesis, Department of Electrical and Computer Engineering, Carnegie Mellon University.

Hähnel, D., Triebel, R., Burgard, W., and Thrun, S. 2002. Map building with mobile robots in dynamic environments. Submitted for publication.

Howard, A. and Kitchen, L. 1996. Generating sonar maps in highly specular environments. In *Proceedings of the Fourth International Conference on Control Automation Robotics and Vision*, pp. 1870–1874.

Konolige, K. and Chou, K. 1999. Markov localization using correlation. In *Proceedings of the Sixteenth International Joint Conference on Artificial Intelligence (IJCAI)*, IJCAI, Stockholm, Sweden.

Kortenkamp, D., Bonasso, R.P., and Murphy, R. (Eds.). 1998. *AI-Based Mobile Robots: Case Studies of Successful Robot Systems*, MIT Press: Cambridge, MA.

Liu, Y., Emery, R., Chakrabarti, D., Burgard, W., and Thrun, S. 2001. Using EM to learn 3D models with mobile robots. In *Proceedings of the International Conference on Machine Learning (ICML)*.

McLachlan, G.J. and Krishnan, T. 1997. *The EM Algorithm and Extensions*. Wiley Series in Probability and Statistics: New York.

Moravec, H.P. 1988. Sensor fusion in certainty grids for mobile robots. *AI Magazine*, 9(2):61–74.

Moravec, H.P. and Elfes, A. 1985. High resolution maps from wide angle sonar. In *Proc. IEEE Int. Conf. Robotics and Automation*, pp. 116–121.

Moravec, H.P. and Martin, M.C. 1994. Robot navigation by 3D spatial evidence grids. Mobile Robot Laboratory, Robotics Institute, Carnegie Mellon University.

Murray, D. and Little, J. 2001. Interpreting stereo vision for a mobile robot. *Autonomous Robots*, to appear.

Neal, R.M. and Hinton, G.E. 1998. A view of the EM algorithm that justifies incremental, sparse, and other variants. In *Learning in Graphical Models*, M.I. Jordan (Ed.), Kluwer Academic Press.

Schiele, B. and Crowley, J. 1994. A comparison of position estimation techniques using occupancy grids. In *Proceedings of the 1994 IEEE International Conference on Robotics and Automation*, San Diego, CA, pp. 1628–1634.

Simmons, R. 1996. Where in the world is xavier, the robot? *Machine Perception*, 5(1).

Simmons, R., Apfelbaum, D., Burgard, W., Fox, M., an Moors, D., Thrun, S., and Younes, H. 2000. Coordination for multi-robot exploration and mapping. In *Proceedings of the AAAI National Conference on Artificial Intelligence*, AAAI, Austin, TX.

Thrun, S. 1993. Exploration and model building in mobile robot domains. In *Proceedings of the IEEE International Conference on Neural Networks*, E. Ruspini (Ed.), IEEE Neural Network Council: San Francisco, CA, pp. 175–180.

Thrun, S. 1998. Learning metric-topological maps for indoor mobile robot navigation. *Artificial Intelligence*, 99(1):21–71.

Thrun, S. 2001. Learning occupancy grids with forward models. In *Proceedings of the Conference on Intelligent Robots and Systems (IROS'2001)*, Hawaii.

Thrun, S., Fox, D., and Burgard, W. 1998. A probabilistic approach to concurrent mapping and localization for mobile robots. *Machine Learning*, 31:29–53. Also appeared in *Autonomous Robots* 5:253–271 (joint issue).

Yamauchi, B. 1997. A frontier-based approach for autonomous exploration. In *Proceedings of the IEEE International Symposium on Computational Intelligence in Robotics and Automation*, Monterey, CA, pp. 146–151.

Yamauchi, B., Langley, P., Schultz, A.C., Grefenstette, J., and Adams, W. 1998. Magellan: An integrated adaptive architecture for mobile robots. Technical Report 98-2, Institute for the Study of Learning and Expertise (ISLE), Palo Alto, CA.

Sebastian Thrun is an Associate Professor of Computer Science and Robotics at Stanford University. Thrun pursues research in artificial intelligence, machine learning, and robotics.